Seismogenic Depth Variation across the Transtensional Northern Walker Lane

Christine J. Ruhl[1,2], Rachel E. Abercrombie[2,3], Rachel Hatch[2], and Kenneth D. Smith[2]

[1]Department of Geosciences, The University of Tulsa, Tulsa, OK, USA

[2]Nevada Seismological Laboratory, University of Nevada, Reno, Reno, NV, USA

[2]Department of Earth and Environment, Boston University, Boston, MA, USA

Corresponding Author: Christine J. Ruhl (cruhl@utulsa.edu)

Key Points:

- High-precision earthquake relocations in the Northern Walker Lane define distinct source zones with complex fault geometries not observed on surface.
- Seismogenic and Moho depths both decrease away from the Sierra Nevada block into the Reno basin, shallowing by ~4 km over ~50 km.
- Constraints on seismogenic depth can be used to refine seismic hazard analysis on a regional basis or for individual faults.

Abstract

We calculate high-precision absolute and relative earthquake relocations to investigate the relationship between seismicity and major active faults, and to explore variation in seismogenic depths across the Northern Walker Lane. We first compute datum-adjusted and station-residual-corrected absolute relocations, before relocating events using waveform cross-correlation. Of 40,581 routinely located earthquakes between 2002 and 2018, we relocate 27,132 (66.9%) with resulting median horizontal and vertical location uncertainties less than ~100 m. We then compute 95th percentile depths as a proxy for seismogenic depth and compare to published Moho depths. Microseismicity occurs in large highly clustered source areas, often consisting of many short, distinct fault structures. Activity concentrates near the ends of mapped Quaternary faults rather than along them. Microseismicity-defined structures in transition zones between major surface faults may identify active fault networks that link faults at the depth. Seismogenic depth shallows away from the Sierra Nevada to the east-northeast over approximately 80 km, from an approximate depth of 17 km to 13 km. This follows, to scale, the decrease in Moho depth across the same region from about 35 km to 30 km. We compare seismogenic and Moho depths to topographic relief and heat flow measurements to discuss controls on the depth of seismicity in the region. Heat flow increases smoothly over the same region of the decreasing seismogenic and Moho depth, increasing by as much as 20 mW/m^2.

Plain Language Summary

We use the similarity between nearby small earthquakes to improve their locations. This highlights important spatial and depth patterns among the events that relate to seismic hazard in the Reno-Tahoe-Carson City area. Seismic activity concentrates near the ends of large mapped surface faults rather than along them. Small earthquakes occur in large, highly clustered source areas, often consisting of many short, distinct fault structures. These planar and linear features occur between major surface faults and may identify active fault networks that link faults at the depth. Across the study region, we compute the depth where 95 percent of the events are shallower than it. This spatially varying depth shallows away from the Sierra Nevada Mountains to the east-northeast over approximately 80 km, from an approximate depth of 17 km to 13 km. We find good spatial agreement between our mid-crustal seismogenic depths and independent estimates for the depth to the base of the lower crust. Both of these depths are controlled by heat flow, which increases across the same region.

Keywords: earthquakes, relocation, seismotectonics

1 Introduction

The seismogenic depth range, over which earthquakes occur, is thought to be the temperature-controlled region in which tectonic deformation occurs by brittle, dynamic failure (*Sibson,* 1982, *Scholz*, 2019). The base of the seismogenic zone is known as the brittle-ductile transition, or locking depth, below which most deformation occurs by more stable aseismic slip (*Scholz*, 2019). The geometry of the seismogenic depth (i.e., basal geometry) is related to crustal strength, seismic hazard, and crustal thermo-mechanical properties and can be inferred from the depth extent of small magnitude and background seismicity (e.g., *Hauksson and Meier,* 2019). Basal geometry can also be used to indicate the locking depth needed for geodetic studies of strain rate (e.g., *Bormann et al.,* 2016) and to estimate the magnitude of future large earthquakes for hazard studies (e.g. *Nazareth and Hauksson,* 2004). Dynamic models show basal geometry can affect whether earthquakes can rupture through stepovers between faults (*Bai and Ampuero,* 2017) and even control the thickness of the fault damage zone (*Ampuero and Mao,* 2017).

Numerous studies have used earthquake locations to infer seismogenic depths in California over the years and relate differences to varying crustal properties (e.g., *Doser and Kanmori,* 1986; *Magistrale and Zhou,* 1996; *Magistrale,* 2002). *Nazareth and Hauksson* (2004) found large variation in basal geometry (10-25 km depth) and compared depth distributions based on moment magnitude, concluding that the depth distributions of background seismicity can be used to infer depths relevant to the extent of larger, more damaging earthquakes. There is also evidence, however, that basal geometry may change over time in response to large earthquakes due to transient strain rates (e.g., *Rolandone et al.,* 2004; *Cheng and Ben-Zion*, 2019). Nonetheless, several authors have shown that variations in seismogenic depth across California correlate strongly with heat flow (e.g., *Zuza and Cao,* 2020) and with yield strength envelopes developed from crustal properties such as heat flow, rock composition, style of faulting, and strain rate (*Hauksson and Meier,* 2019).

While seismogenic thickness across California has been well studied using high-precision earthquake relocations (e.g., *Hauksson and Meier,* 2019; *Siler et al.,* 2019), no such studies exist in the adjacent Walker Lane using seismicity relocated with regional network data in Nevada. Understanding seismogenic depth is important in the Walker Lane where high strain rates (*Hammond and Thatcher,* 2007) are accommodated across large and discontinuous fault zones (e.g., *Wesnousky,* 2005) with high and highly variable heat flow (e.g., *Siler et al.,* 2019). Here, we explore the seismogenic depth, Moho depth, and heat flow variation across the Northern Walker Lane near the populated Reno-Tahoe-Carson City area (Figure 1).

The Walker Lane (WL) is a transtensional zone between the relatively stable Sierra Nevada block to the west and the extensional Basin and Range province to the east (Figure 1 inset). It is well-defined geomorphologically as a 100 to 300 km wide, northwest-trending belt of diverse topography and discontinuous strike-slip and normal faulting (*Stewart,* 1988). North of Lake Tahoe, the Walker Lane accommodates as much as 10 mm/yr of dextral shear related to the Pacific-North America plate boundary (*Hammond and Thatcher,* 2007), but geodetic slip rate estimates for individual Quaternary surface faults are inconsistent with geologic slip rates based on paleoearthquake studies (e.g., *Gold et al.,* 2014). The discrepancy in slip rates suggests that distributed deformation across unidentified fault structures plays an important role in accommodating strain across the Northern Walker Lane (*Gold et al.,* 2014). This is further supported by observations of distributed microseismicity and significant earthquakes occurring between, around, and across mapped surface faults (*Ruhl, Seaman, et al*., 2016). The relationship between microseismicity and large active faults is not well understood, especially in discontinuous fault zones with low individual fault slip rates. It is possible that seismicity occurring near the ends of faults and in stepovers between them are highlighting fault networks that would enable multiple-fault ruptures like the 1992 M_w7.3 Landers, California earthquake (e.g., *Hauksson et al.,* 1993). High-precision earthquake relocations may help identify fault structures within these transition zones and illuminate their relationship to surface faults.

Characterized by abundant microseismicity and a history of moderate magnitude (M5-7) earthquakes, the Walker Lane is a natural laboratory for exploring the relationship between microseismicity, active faulting, and crustal properties. Numerous hot springs (>150° F), including operational geothermal fields (>200° F), exist in the Reno-Tahoe-Carson City area (*Garside and Schilling*, 1979). Ongoing, extensive microseismicity, including many seismic swarms, is commonplace in Nevada and parts of eastern California (e.g., Eastern California Shear Zone, Salton Trough) and often occurs away from mapped surface faults (e.g., Lake Tahoe faults) or perpendicular to them (e.g., Mohawk Valley fault, Polaris fault) (Figure 2). Background seismicity therefore provides key information about the crust including but not limited to stress orientations, rates of microseismicity, seismogenic depths, and identifying active subsurface fault structures. Here, we develop a high precision relocated earthquake catalog to characterize seismogenic depths across the region and to analyze microseismicity patterns related to mapped surface faults. Our goal is to understand the current seismotectonic behavior of this complex transition zone, and its implications for seismic hazard in the populated Reno-Tahoe-Carson City region (Figure 2).

1.1 Tectonic Setting of the Northern Walker Lane

Our study region is located between the Sierra Nevada mountains and the Basin and Range province; it extends along the California-Nevada border from approximately 38.5N to 40.5N and includes the populated Reno-Tahoe-Carson City corridor (see Figure 1). The Sierra Nevada is considered a stable block with little internal deformation, as shown by a lack of

Quaternary faulting (west side of Figure 1). The Basin and Range province, on the other hand, is characterized by middle to late Cenozoic extension accommodated on north- and northeast-striking range-bounding normal faults that form a series of basins from Reno, NV to Salt Lake City, UT (*Stewart,* 1998; *Dickinson,* 2006). In the transition from the Sierra Nevada block to the Basin and Range, there exists a complex zone of transtensional deformation defined as the Walker Lane (*Stewart,* 1988).

GPS velocities (e.g., *Bennett et al.,* 2003; *Hammond and Thatcher,* 2007) show that the Sierra Nevada block is moving northwest with respect to North America at a higher rate (up to ~10 mm/yr) than the Basin and Range; this promotes dextral shear within the Walker Lane. Numerous geodetic and geologic studies suggest that the Walker Lane is a significant part of the Pacific-North America plate boundary system and accommodates up to 25% of relative plate motion through a wide, discontinuous zone of faulting centered roughly along the California-Nevada border (*Stewart,* 1988; *Thatcher et al.,* 1999; *Dixon et al.,* 2000; *Hammond et al.*, 2011; and *Busby,* 2013). Relative motion estimates decrease northward across our study area from ~10 mm/yr to ~7 mm/yr between 38° and 41° N (*Hammond and Thatcher,* 2007).

The Walker Lane is generally split into three segments: Southern, Central, and Northern. The Southern Walker Lane, including the area of the 2019 Ridgecrest, CA earthquakes, is a continuation of the Eastern California shear zone (ECSZ), extending north of the Garlock fault. Like the ECSZ, it is characterized by well-defined right-lateral faults with upwards of 50 km right-lateral offset (*Wesnousky,* 2005), but cumulative right-lateral displacement decreases northward into the Central Walker Lane (> 34 km) and the Northern Walker Lane (20-30 km). Mapped strike-slip faults decrease in length and are less well defined in these areas as compared to the Southern Walker Lane (*Wesnousky,* 2005). The faulting style also changes; Central Walker Lane deformation is accommodated on a westward-evolving set of *en echelon* normal faults that transitions into the Northern Walker Lane in the southern part of the study area (Figure 1; *Wesnousky,* 2005; *Surpless,* 2008; *Wesnousky et al.,* 2012).

In the study region, left-stepping east-dipping normal faults define the eastern edge of the Sierra Nevada block as far north as the Lake Tahoe basin (Figure 1). Continuing northeastward through the North Lake Tahoe area, there are several right-stepping, down-to-the-east normal faults extending eastward to the Mount Rose fault zone (MRFZ, Figure 2) in the Reno-Carson City corridor. North of Lake Tahoe, deformation is again accommodated on mostly strike-slip faults. North and northwest of the Mount Rose fault zone, the major structures are northwest-striking dextral or northeast-striking sinistral faults. The northeast-striking Dog Valley fault zone (DVFZ) crosses the recently identified northwest-striking Polaris fault zone (PFZ; *Hunter et al.,* 2011). Dextral faulting continues northwest of the Polaris fault on the northwest-striking Mohawk Valley fault zone (MVFZ; *Hunter et al.,* 2011; *Gold et al.,* 2014).

Low slip rates (0.1 to 3 mm/yr) on individual faults in the Northern Walker Lane and Basin and Range make assessing seismic hazard from surface faults alone difficult due to the degradation of surface features over long recurrence times. Another complication is that much of the seismicity tends to occur in between, away from, or perpendicular to the major faults (Figure 2; *Ruhl, Seaman, et al., 2016*). Inconsistencies between geodetic slip rates and geologic slip rates are often attributed to distributed deformation on unidentified structures (e.g., *Gold et al.,* 2014); this remains, however, an important unresolved aspect of seismic hazard for the Northern Walker Lane. Thus, providing motivation for studying microseismicity that might highlight areas of subsurface, obscured, or unidentified faults. We further summarize recent paleoseismic studies (Section S1.1) and significant historical earthquakes (Section S1.2; labeled in Figure 1) in and around our study area in the Supporting Information.

2 Analysis: Seismic Data and Earthquake Relocation

We use earthquake origin and arrival time information developed at the Nevada Seismological Laboratory (NSL) in routine event analysis between 1 Jan. 2002 and 31 Dec. 2019. Seismicity prior to 2002 is not used due to incompleteness associated with poorer station coverage and station quality (i.e., analog). We limit our analysis to hypocenters in the NSL catalog with at least 8 defining phases (i.e., 8 P- and/or S-phase arrival times).

Our initial catalog includes 40,581 earthquake locations (Figure S1) and origin times (x_0, y_0, z_0, t_0) with approximately 700,000 total arrival times at up to 112 seismic stations within 100 km (Figure 1). We implement the routinely used, USGS-supported earthquake location program HYPOINVERSE-2000 (*Klein,* 1978; *Klein,* 2002) to relocate the data using our preferred velocity model. We use a 1-D, flat-earth velocity model (Table S2), and calculate depths relative to the average station elevation. Because of high regional relief, we apply a datum correction on a station-by-station basis to each P- and S-arrival time based on a compressional wave speed of 3.5 km/s across the distance between the station elevation and the mean elevation. After running HYPOINVERSE-2000 with adjusted travel times, we calculate the average station residuals for P- and S-phase arrivals, apply those to the data, and perform a final inversion for absolute locations following *Ruhl, Seaman, et al.* (2016), shown in Figure 2a. This step is intended as a correction for variations in the 3-D velocity field that are not accounted for in our simple 1-D model.

Next, we apply the relative relocation algorithm GrowClust (*Trugman and Shearer*, 2017), which is a hybrid hierarchical clustering algorithm that groups and relocates events within similar event clusters based on waveform cross-correlation coefficients. GrowClust uses the average location of the centroid of the cluster for its reference location. This method uses the L1 norm rather than the least-squares inversion for standard matrix inversion. The L1 norm is less sensitive to outliers and has been shown in some studies (*Shearer,* 1997) to return higher-quality solutions. We filter waveforms from 1-10 Hz before cross-correlating all events with their 700 nearest neighbors. We process P- and S-wave arrivals separately, cross-correlating P- and S-waves with time windows starting 1.0 before and ending 2.0 and 4.0 seconds after each arrival, respectively. Applying a cross-correlation threshold of 0.6 and requiring at least 10 common phases results in over 1.9M phase pairs. GrowClust uses a bootstrapping method to estimate location uncertainties (Figure S2). Of 40,581 routinely located earthquakes, we relocated 27,132 (66.9%), shown in Figure 2b. Horizontal and vertical uncertainties are less than 0.27 and 0.51 km, respectively, for 95% of all relocated events. Comparison maps and cross-sections of the NSL catalog and GrowClust relocations are shown in Figure S3.

3 Results and Discussion

The high precision earthquake relocations that we obtain reveal significant variation in the basal geometry of the seismogenic zone, and in the seismicity-defined fault structures across the Sierra Nevada-Walker Lane transition. First, we discuss the spatial patterns observed in crustal seismicity with respect to the active surface faults (Section 3.1, Figure 2). Next, we characterize overall depth distributions by time, magnitude, and moment release (Section 3.2,

Figure 3), showing that seismogenic depth and Moho depth both shallow to the east-northeast (Figure 4). We compare these systematic changes to corresponding increases in heat flow models (Section 3.3, Figure 4). Finally, we discuss b-value variation with depth (Section 3.4, Figure 3) and the possibility of time-dependent changes in basal geometry after two large (M5+) earthquakes.

3.1 Distribution of Crustal Seismicity with respect to Active Faults

Seismicity is occurring in tightly defined spatiotemporal and spatial clusters that appear to define small planar faults. These structures concentrate north of Lake Tahoe in three main zones with distinct seismicity-defined fault patterns (Figure 2). The first zone follows the Mohawk Valley and Polaris fault zones, extending northwest from north Lake Tahoe (MVFZ & PFZ, Figure 2). The second zone extends east-northeast from north Lake Tahoe into the Reno Basin, connecting the first and third zones. The third zone trends northwest from the Mount Rose fault zone and parallels the Mohawk Valley and Polaris fault zones. These source zones were originally identified and described by *Ruhl, Seamen, et al.* (2016). Together, they outline an area without significant seismicity that trends northwest between the zones. The absence of seismicity is especially apparent on the northeast-trending Dog Valley fault zone (DVFZ; Figure 2).

Seismicity is also absent along major normal faults from the Lake Tahoe-bounding faults to the Mount Rose fault zone (Figures 1 and 2). Instead, seismicity is concentrated at the ends of normal faults (e.g., northern extent of the normal faults in the Lake Tahoe basin) and in the transitions between distinct fault zones (e.g., *Ichinose et al.,* 1998; Figure 2). These regions between large mapped faults are those in which *Crider and Pollard* (1998) found increased stresses in numerical models. Including the small structures revealed by the seismicity in future models could help to inform probabilities of a single earthquake rupturing multiple mapped faults in the region (e.g. *Madden et al.,* 2013). A lack of seismicity on the primary range-bounding faults, and perhaps the Dog Valley fault zone, implies that they may behave with a characteristic recurrence in which principal moment release is accounted for in a small number of large magnitude earthquakes (e.g., *Ichinose et al.,* 1998) rather than following a Gutenberg-Richter magnitude relationship over long time periods. An alternative explanation for quiescence on major surface faults could be that past large earthquakes ruptured below the seismogenic zone as suggested and simulated by, e.g., *Jiang and Lapusta* (2016), for strike-slip faults in Southern California.

The 1966 M_L 5.9 Truckee, CA earthquake (Event 11, Figure 1) is among the most notable historic earthquakes in the study region. It occurred near the intersection of the northwest-striking Polaris and the northeast-striking Dog Valley fault zones. The 1966 event was interpreted as a northeast-striking, left-lateral rupture conjugate to the major northwest-striking, right-lateral faults (e.g., *Tsai and Aki.,* 1970). Aftershocks of the 1966 earthquake may still be present in the recent catalog; however, the central and northeast sections of the Dog Valley fault zone lack seismicity in the instrumental record as noted above.

Another notable earthquake in this area, is the Nov. 1995 M_w 4.5 Border Town earthquake (Event 15, Figure 1). This north-northeast-striking, down-to-the-west, high-angle normal-faulting event was felt throughout the Reno area (*Ichinose et al.,* 1997). Investigations of historically felt earthquakes from the late 1800s to early 1900s (*dePolo et al.,* 1997) suggest that there are additional moderate magnitude events that likely occurred near this event, but their locations are highly uncertain (e.g., Events 5, 7, 9 on Figure 1; Table S1). The longest and most obvious spatiotemporal seismicity cluster in our relocations is the 2008 Mogul earthquake sequence that occurred just west of the Reno Basin (Figure 2). This earthquake ruptured a previously unknown fault that crosses short, discontinuous mapped normal faults. Two months of foreshock activity led to an unusually shallow (< 4 km) M_W 5.0 mainshock on 26 Apr. 2008. Relocations of the sequence define an ~8-km, northwest-striking trend in seismicity (*von Seggern et al.,* 2015; *Ruhl, Abercrombie, et al.,* 2016), which accommodated right-lateral motion interpreted from moment tensors developed for the largest events (*Ruhl, Abercrombie, et al.,* 2016). The relocations obtained in this regional study match well the double-difference relocations of *Ruhl, Abercrombie, et al.* (2016) and *von Seggern et al.* (2015). *Bell et al.*, (2012) suggested that this sequence represents a northwestward migration of the Walker Lane. In other words, they interpret that north-striking normal faults in the Reno basin associated with Basin and Range extension are being overprinted with dextral shear from the Walker Lane.

Small San Andreas fault-parallel and fault-conjugate seismicity lineaments occur throughout the area. For example, along the Mohawk Valley and Polaris fault zones, seismicity clusters in distinct lineaments that strike both parallel to and nearly orthogonal to the fault strikes. None of the northwest-striking seismicity occurs directly on the near-vertical surface faults, but rather in an approximately 5 km-wide zone around the fault traces. Seismicity is concentrated at the southern end of the Polaris fault zone, at the intersection of the Dog Valley and Polaris fault zones, and in the discontinuous step-over zone between the Polaris and Mohawk Valley fault zones (*Hatch et al.*, 2018). In the east-west trending seismicity zone north of Lake Tahoe, seismicity lineaments trend north-northwest in an *en echelon* pattern, with some east-northeast-striking, intersecting conjugates. In the eastern seismicity zone, north and south of the Mogul sequence, microseismicity clusters trend predominantly to the north-northeast. Many of the well-defined seismicity structures are steeply-dipping and subvertical as seen in vertical cross-sections oriented parallel to each source zone (Figure S3). The alignment of these features may support the development of an incipient, high-seismicity fault zone. This is supported by a history of earthquakes greater than M5 as previously suggested by, e.g., *dePolo et al.* (1997).

Orthogonal faulting, as seen on a small scale here, has become an increasingly common observation in large-magnitude strike-slip earthquakes in the western US (e.g., *Ross et al.*, 2019, *Smith et al.*, 2020, 08). Laboratory experiments suggest that conjugate faults should be oriented 60° from their counterparts (e.g., *Twiss and Moores,* 1992), however orthogonal strike-slip conjugates are often observed in nature (e.g., *Kilb and Rubin,* 2002). Bookshelf-style block rotation between parallel strike-slip faults and low frictional properties are among mechanisms proposed for these observations. Considering their orientation and proximity to the Sierra Nevada block, one possible interpretation is that these are tensile fractures associated with the relatively weak faulted terrains bordering the competent, stable granitic block. Another possibility is that abundant seismicity, including fault-perpendicular features, is a common feature of young, developing strike-slip fault systems like the Northern Walker Lane.

3.2 Depth Distribution of Crustal Seismicity

Next, we characterize the depth of seismicity with respect to time, magnitude, and moment release (Figure 3). While most of the microseismicity in this region occurs shallower than ~20 km depth, two lower-crustal (30-35 km depth) earthquake swarms took place near north Lake Tahoe in 2003-2004 (*Smith et al.,* 2004), and near Sierraville, CA in 2011-2012 (*Smith* *et al.,* 2016; Figures 1, 2, and 3). These low-magnitude sequences occurred beneath, and are aligned with, the eastern edge of the Sierra Nevada block. They are interpreted as magmatic or fluid injection events at the Moho-Lower Crust transition (*Smith et al.,* 2016). Both are associated with increases in upper crustal seismicity rates, including a 15-km depth M4.7 earthquake concurrent with the 2011 swarm (*Smith et al.,* 2016). We also highlight the unusually shallow Mogul earthquake swarm which dominates the seismicity in the 0-5 km range (Figure 3a). This sequence occurred on an unmapped fault as discussed in Section 3.1 and had significant amounts of shallow aseismic slip (*Bell et al.,* 2012; *Ruhl, Abercrombie, et al*., 2016).

The depth distribution is magnitude independent, i.e., small and moderate earthquakes happen across all shallow crustal depth ranges (Figures 3b and 3c). However, we do note that the majority of seismic moment release occurs at the base of the seismogenic zone around 17 km (Figure 3d). Because our relocations include both GrowClust relocated events and Hypoinverse absolute relocations, we repeat the analysis in Figure 3 using only the cross-correlated events (i.e., the best-located events, Figure S4); we find the results to be indistinguishable.

We also investigate whether there is any temporal change in seismogenic depth in the region, as observed following large earthquakes elsewhere *by Rolandone et al. (*2004) and *Cheng and Ben-Zion* (2019). We apply similar approaches to two well-recorded sequences with the largest magnitude events, but found we had an insufficient number of earthquakes to observe any statistically significant changes between different time windows. Furthermore, if the increase in seismogenic depth is magnitude-dependent (e.g., *Zielke et al.,* 2020), then these earthquakes, that are unlikely to have ruptured through the seismogenic zone, are also perhaps too small to effect basal geometry (<M6.0).

3.3 Comparing Seismogenic Depth to Crustal Properties: Moho Depth and Heat Flow

To explore crustal structure, we calculate the 95th percentile of depth (d95) as a proxy for seismogenic depth across the region. Using non-overlapping 0.1x0.1-degree bins with at least three events, we calculate the smoothed d95 results shown in Figure 4a. We use a series of east-northeast-striking and northwest-striking profile lines (Figure S5) to explore the variation across the region, two of which are shown in Figure 4. In general, seismogenic depths shallow from west to east across the region: from ~17 km along the boundary between the Sierra Nevada and the Walker Lane to ~13 km within the Reno-Carson City corridor (Figure 4c; Figure S6). It is expected that the competent, high-elevation granites of the Sierra Nevada would have a deeper brittle-ductile transition that supports seismogenic behavior at greater depths.

We compare our calculated seismogenic depths to the surface topography (Figures 4c, S5-7) and to Moho depths derived from receiver function analysis by *Frasetto et al.* (2011; Figures 4d, S5-7) for ten SW-to-NE profile lines (Figures 4 and S5) and ten NW-to-SE profile lines (Figures S5 & S6). The visual correlation between Moho depth and seismogenic depth is quite striking. The Moho sits approximately 20 km below the base of the seismogenic crust, but correlation decreases towards the east - especially near the northern end of Pyramid Lake. The Moho shallows significantly while the seismogenic depth gets deeper. This is evident in all cross-sections shown in Figure S5 towards the right (eastern) side of the profile lines as well as in Figures S7a through S7c. This mismatch could be related to geothermal activity, although this is also closer to the edge of the crustal structure model of *Frasetto et al.* (2011) where uncertainties are higher. Additionally, there are fewer earthquakes in that part of our study region and therefore the seismogenic depths are also more uncertain.

Heat flow measurements from *Williams and DeAngelo* (2011) increase eastward across the study region from approximately 50 mW/m^2 to 90 mW/m^2 (Figures 4, S5 – S7). Spatial variation in heat flow correlates with both seismogenic depths and Moho depths, especially from southwest-to-northeast across the Sierra Nevada-Walker Lane transition. *Hauksson and Meier* (2019) compared seismogenic depth distributions to yield strength envelopes derived from heat flow for different crystalline rock types in the various lithotectonic blocks across southern California. Seismogenic depth (d95) varies from over 20-km depth in the western Sierra Nevada block to approximately 12-km and 9-km depth in the eastern Sierra Nevada and Southern Walker Lane blocks, respectively (*Hauksson and Meier*, 2019). The Southern Walker Lane block has the second highest heat flow and shallowest d95 reported in their study. This shallowing of 3-4 km across the Sierra Nevada-Southern Walker Lane boundary is similar to our observations in the Northern Walker Lane.

Because the base of the seismogenic zone controls the area of potential earthquake ruptures, and therefore maximum earthquake magnitude, it is an important factor for earthquake hazard assessment. For example, for a shear modulus of 3.2 GPa, rupture length of 35 km (e.g., the entire Polaris fault), and 5 m of slip, an increase in seismogenic depth of 5 km corresponds to an increase in fault area of 175 km^2 and an increase in seismic moment of 5.6 x 10^{18} Nm. This is equivalent to an increase in estimated maximum magnitude for the Polaris fault from 6.7 to 6.8, using the moment magnitude relation. Increases would be more significant for dipping faults, such as the prevalent range-bounding normal faults, especially if listric geometries were present. The relocated catalog developed in this study can be used to characterize fault geometries at depth (see Acknowledgements and Data).

3.4 Frequency-Magnitude Variation with Depth

We calculate b-value variation with depth using a maximum likelihood approximation (Figure 3c and Figure S8). We divide the data into non-overlapping 2.5 km depth bins each with several hundred events or more. Unsurprisingly, the b-value of lower crustal seismicity related to the injection swarms is significantly higher than the upper crustal b-values. This is consistent with the higher b-values found in areas of volcanic and magmatic regions (*Mogi,* 1963). We observe a slight decrease in b-value with depth for upper crustal seismicity consistent with the findings of *Mori and Abercrombie* (1997) and *Gerstenberger* et al. (2001). *Amorese* et al. (2010) saw a similar trend but suggested it may not be resolvable. Since then, *Spada et al.* (2013) and *Petruccelli et al.* (2019) also reported decreasing b-value with depth. This trend may also be related to seismogenic width and the strength of the crust (i.e., b-value decreases linearly with increasing differential stress; Scholz, 2015).

4 Conclusions

Seismicity in the Reno-Tahoe-Carson City region accommodates the structural transition between normal faulting along the eastern Sierra Nevada block to the south into the dextral faults of the Northern Walker Lane along the northeast Sierra Nevada range-front. We relocate earthquakes between 2002 and 2019 and reveal small-scale seismicity structures distributed in three distinct source zones. Using high precision relocated seismicity with resulting median horizontal and vertical location uncertainties less than ~100 m, we quantified seismogenic depth across the study area and compared it to published Moho depths and heal flow measurements.

Seismogenic depth shallows away from the Sierra Nevada to the east-northeast, from approximately 17 km to 13 km depth. This follows, to scale, the decrease in Moho depth across the same region from about 35 km to 30 km. Microseismicity occurs in highly clustered source areas, often consisting of many short, distinct fault structures. Activity concentrates near the ends of mapped Quaternary faults rather than along them. Microseismicity-defined structures in transition zones between major surface faults may help identify active fault networks that link faults at the depth.

5 Acknowledgements and Data

We thank the field technical staff, network systems staff, and data analysis team at the Nevada Seismological Laboratory for maintaining the network, software systems, and regional earthquake and phase database used here. NSL data collection and network operations support for this study was provided through a Cooperative Agreement with the U.S. Geological Survey for regional seismic network operations and the State of Nevada. We accessed waveforms through IRIS Data Services, specifically the IRIS Data Management Center (DMC), using ObsPy, a python library for seismological analysis (Krischer et al., 2015). The ANSS historical earthquake catalog data for this study were accessed through the Northern California Earthquake Data Center (NCEDC), doi:10.7932/NCEDC. *U.S. Geological Survey and New Mexico Bureau of Mines and Mineral Resources, Quaternary fault and fold database for the United States, accessed February 11, 2020, at:* https://www.usgs.gov/natural-hazards/earthquake-hazards/faults. Our relocated earthquake catalog is available through Zenodo (*Ruhl et al.,* 2020) at the following link: https://zenodo.org/record/4141086.

6 References

Amorese, D., Grasso, J. R., & Rydelek, P. A. (2010). On varying b-values with depth: results from computer-intensive tests for Southern California. *Geophysical Journal International*, *180*(1), 347-360.

Ampuero, J. P., & Mao, X. (2017). Upper limit on damage zone thickness controlled by seismogenic depth. Fault zone dynamic processes: Evolution of fault properties during seismic rupture, 227, 243.

Bai, K., & Ampuero, J. P. (2017). Effect of seismogenic depth and background stress on physical limits of earthquake rupture across fault step overs. Journal of Geophysical Research: Solid Earth, 122(12), 10-280.

Bell, J. W., F. Amelung, and C. D. Henry (2012), InSAR analysis of the 2008 Reno-Mogul earthquake swarm: Evidence for westward migration of Walker Lane style dextral faulting, *Geophys. Res. Lett.* 39, 18.

Bennett, R. A., Wernicke, B. P., Niemi, N. A., Friedrich, A. M., & Davis, J. L. (2003). Contemporary strain rates in the northern Basin and Range province from GPS data. *Tectonics*, *22*(2).

Bormann, J. M., Hammond, W. C., Kreemer, C., & Blewitt, G. (2016). Accommodation of missing shear strain in the Central Walker Lane, western North America: Constraints from dense GPS measurements. *Earth and Planetary Science Letters*, *440*, 169-177.

Busby, C. J., Hagan, J. C., & Renne, P. (2013). Initiation of Sierra Nevada range front–Walker Lane faulting ca. 12 Ma in the Ancestral Cascades arc. *Geosphere*, *9*(5), 1125-1146.

Cheng, Y., & Ben-Zion, Y. (2019). Transient brittle-ductile transition depth induced by moderate-large earthquakes in southern and Baja California. *Geophysical Research Letters*, *46*(20), 11109-11117.

Crider, J. G., & Pollard, D. D. (1998). Fault linkage: Three-dimensional mechanical interaction between echelon normal faults. Journal of Geophysical Research: Solid Earth, 103(B10), 24373-24391.dePolo, C. M., J. G. Anderson, D. M. dePolo, and J. G. Price (1997), Earthquake Occurrence in the Reno-Carson City Urban Corridor, Seism. Res. Lett. 68, 401-412.

Dickinson, W. R. (2006). Geotectonic evolution of the Great Basin. Geosphere, 2(7), 353-368.

Dixon, T. H., Miller, M., Farina, F., Wang, H., & Johnson, D. (2000). Present-day motion of the Sierra Nevada block and some tectonic implications for the Basin and Range province, North American Cordillera. Tectonics, *19*(1), 1-24.

Doser, D. I., & Kanamori, H. (1986). Depth of seismicity in the Imperial Valley region (1977–1983) and its relationship to heat flow, crustal structure and the October 15, 1979, earthquake. *Journal of Geophysical Research: Solid Earth*, *91*(B1), 675-688.

Frasetto, A. M., G. Zandt, H. Gilbert, T. J. Owens, and C. H. Jones (2011), Structure of the Sierra Nevada from receiver functions and implications for lithospheric floundering, *Geosphere* 7 (4), 898 – 921.

Garside L. J. and J. H. Schilling (1979) Thermal Waters of Nevada, Nevada Bureau of Mining and Geology Bulletin 91, 167 pp.

Gerstenberger, M., Wiemer, S., & Giardini, D. (2001). A systematic test of the hypothesis that the b value varies with depth in California. *Geophysical Research Letters*, *28*(1), 57-60.

Gold, R. D., Briggs, R. W., Personius, S. F., Crone, A. J., Mahan, S. A., & Angster, S. J. (2014). Latest Quaternary paleoseismology and evidence of distributed dextral shear along the Mohawk Valley fault zone, northern Walker Lane, California. *Journal of Geophysical Research: Solid Earth*, *119*(6), 5014-5032.

Hammond, W. C. and W. Thatcher (2007), Crustal deformation across the Sierra Nevada, northern Walker Lane, Basin and Range transition, western United States measured with GPS, 2000–2004, *J. Geophys. Res.* 112 (B5); doi: 10.1029/2006JB004625.

Hammond, W. C., G. Blewitt, and C. Kreemer (2011), Block modeling of crustal deformation of the northern Walker Lane and Basin and Range from GPS velocities, *J. Geophys. Res.* 116 (B4); doi: 10.1029/2010JB007817.

Hatch, R. L., R. E. Abercrombie, and C. J. Ruhl and K. D. Smith (2018), Earthquake Interaction, Fault Structure, and Source Properties of a Small Sequence in 2017 near Truckee, *Bull. Seism. Soc. Am.,* doi:10.1785/0120180089.

Hauksson, E., Jones, L. M., Hutton, K., & Eberhart-Phillips, D. (1993). The 1992 Landers earthquake sequence: Seismological observations. *Journal of Geophysical Research: Solid Earth*, *98*(B11), 19835-19858.

Hauksson, E., & Meier, M. A. (2019). Applying depth distribution of seismicity to determine thermo-mechanical properties of the seismogenic crust in Southern California: comparing lithotectonic blocks. *Pure and Applied Geophysics*, 176(3), 1061-1081.

Hunter, L. E., Howle, J. F., Rose, R. S., & Bawden, G. W. (2011). LiDAR-Assisted Identification of an Active Fault near Truckee, CaliforniaLiDAR-Assisted Identification of an Active Fault near Truckee, California. *Bulletin of the Seismological Society of America*, *101*(3), 1162-1181.

Ichinose, G. A., K. D. Smith, and J. G. Anderson (1997), Source parameters of the 15 November 1995 Border Town, Nevada, earthquake sequence, *Bull. Seism. Soc. Am.* 87 (3), 652-667.

Ichinose, G., J. Anderson, K. Smith, D. dePolo, R. Anooshehpoor, R. Schweickert, and M. Lahren (1998), The Seismotectonics of the 30 October 1998 Incline Village, Nevada Earthquake and Its Effects, *Seism. Res. Lett.* 70 (3), 297 – 305.

Jiang, J., & Lapusta, N. (2016). Deeper penetration of large earthquakes on seismically quiescent faults. Science, 352(6291), 1293-1297.

Kilb, D., and A. M. Rubin (2002), Implications of diverse fault orientations imaged in relocated aftershocks of the Mount Lewis, M_L 5.7, California, earthquake, *J. Geophys. Res.* 107 (B11); doi: 10.1029/2001JB000149.

Klein, F.W. (1978), Hypocenter locations program HYPOINVERSE: US Department of the Interior, Geological Survey.

Klein, F. W. (2002), User's guide to HYPOINVERSE-2000, a Fortran program to solve for earthquake locations and magnitudes (No. 2002-171). US Geological Survey.

Krischer, L., Megies, T., Barsch, R., Beyreuther, M., Lecocq, T., Caudron, C., & Wassermann, J. (2015). ObsPy: A bridge for seismology into the scientific Python ecosystem. Computational Science & Discovery, 8(1), 014003.

Madden, E. H., Maerten, F., & Pollard, D. D. (2013). Mechanics of nonplanar faults at extensional steps with application to the 1992 M 7.3 Landers, California, earthquake. Journal of Geophysical Research: Solid Earth, 118(6), 3249-3263.

Magistrale, H. (2002). Relative contributions of crustal temperature and composition to controlling the depth of earthquakes in southern California. *Geophysical research letters*, *29*(10), 87-1.

Magistrale, H., & Zhou, H. W. (1996). Lithologic control of the depth of earthquakes in southern California. *Science*, *273*(5275), 639-642.

Mogi, K. (1963), Some discussions on aftershocks, foreshocks, and earthquake swarms--The fracture of a semi-infinite body caused by an inner stress origin and its relation to the earthquake phenomena. 3, *Bull. Earthquake Res. Inst. Tokyo Univ.*, 41, 615-658, 1963.

Mori, J., & Abercrombie, R. E. (1997), Depth dependence of earthquake frequency-magnitude distributions in California: Implications for rupture initiation. *J.Geophys. Res. Solid Earth*, 102(B7), 15081-15090.

Nazareth, J. J., & Hauksson, E. (2004). The seismogenic thickness of the southern California crust. Bulletin of the Seismological Society of America, 94(3), 940-960.

Petruccelli, A., Gasperini, P., Tormann, T., Schorlemmer, D., Rinaldi, A. P., Vannucci, G., & Wiemer, S. (2019), Simultaneous dependence of the earthquake-size distribution on faulting style and depth. Geophys. Res. Lett., 46, 11,044–11,053. https://doi-org.ezproxy.b2u01.e9dGuL/1008.31909279.

Rolandone, F., Bürgmann, R., & Nadeau, R. M. (2004). The evolution of the seismic-aseismic transition during the earthquake cycle: Constraints from the time-dependent depth distribution of aftershocks. *Geophysical Research Letters*, *31*(23).

Ross, Z. E., Idini, B., Jia, Z., Stephenson, O. L., Zhong, M., Wang, X., ... & Hauksson, E. (2019). Hierarchical interlocked orthogonal faulting in the 2019 Ridgecrest earthquake sequence. *Science*, *366*(6463), 346-351.

Ruhl, C. J., R. E. Abercrombie, K. D. Smith, and I. Zaliapin (2016), Complex spatiotemporal evolution of the 2008 Mw 4.9 Mogul earthquake swarm (Reno, Nevada): interplay of fluid and faulting, *J. Geophys. Res. Solid Earth, 121,* doi:10.1002/2016JB013399.

Ruhl, C. J., T. C. Seaman, K. D. Smith, and G. M. Kent (2016), Seismotectonic and seismic hazard implications for the Reno-Tahoe area of the Walker Lane in Nevada and California from relocated seismicity, first-motion focal mechanisms, moment tensors, and variations in the stress field, in Applied Geology in California, *AEG Special Volume*, eds. R. Anderson and H. Ferriz.

Ruhl, Christine J., Abercrombie, Rachel, Hatch, Rachel, & Smith, Kenneth. (2020). Relocated Earthquake Catalog - Seismogenic Depth Variation across the Transtensional Northern Walker Lane (Version 1.0) [Data set]. Zenodo. http://doi.org/10.5281/zenodo.4141086.

Scholz, C. H. (2015), On the stress dependence of the earthquake b value, *Geophys. Res. Lett.*, 42, 1399–1402, doi:10.1002/2014GL062863.

Scholz, C. H. (2019). The mechanics of earthquakes and faulting. Cambridge university press.

Shearer, P. M. (1997). Improving local earthquake locations using the L1 norm and waveform cross correlation: Application to the Whittier Narrows, California, aftershock sequence. *Journal of Geophysical Research: Solid Earth*, *102*(B4), 8269-8283.

Sibson, R. H. (1982). Fault zone models, heat flow, and the depth distribution of earthquakes in the continental crust of the United States. *Bulletin of the Seismological Society of America*, 72(1), 151-163.

Siler, D. L., Faulds, J. E., Hinz, N. H., Dering, G. M., Edwards, J. H., & Mayhew, B. (2019). Three-dimensional geologic mapping to assess geothermal potential: examples from Nevada and Oregon. *Geothermal Energy*, *7*(1), 1-32.

Smith, K., Hatch, R. L., Ruhl, C. J., & Abercrombie, R. E. (2020, 08). Order and timing of high-angle conjugate strike-slip faulting in Walker Lane sequences. Poster Presentation at 2020 SCEC Annual Meeting.

Smith, K. D., D. von Seggern, G. Blewitt, L. Preston, J. G. Anderson, B. P. Wernicke, and J. L. Davis (2004), Evidence for deep magma injection beneath Lake Tahoe, Nevada-California, *Science* 305 (5688), 1277-1280.

Smith, K. D., G. M. Kent, D. P. von Seggern, N. W. Driscoll, and A. Eisses (2016), Evidence for Moho-lower crustal transition depth diking and rifting of the Sierra Nevada microplate, *Geophys. Res. Lett.*, 43, doi:10.1002/2016GL070283.

Spada, M., Tormann, T., Wiemer, S., & Enescu, B. (2013). Generic dependence of the frequency-size distribution of earthquakes on depth and its relation to the strength profile of the crust. *Geophys. Res. Lett.*, 40(4), 709-714.

Stewart, J. H. (1988), Tectonics of the Walker Lane Belt, Western Great Basin: Mesozoic and Cenozoic Deformation in a Zone of Shear, *Metamorphism and crustal evolution of the western United States*, 7, p. 683-713.

Surpless, B. (2008). Modern strain localization in the central Walker Lane, western United States: Implications for the evolution of intraplate deformation in transtensional settings. *Tectonophysics*, *457*(3-4), 239-253.

Thatcher, W., Foulger, G. R., Julian, B. R., Svarc, J., Quilty, E., & Bawden, G. W. (1999). Present-day deformation across the Basin and Range province, western United States. *Science*, *283*(5408), 1714-1718.

Trugman, D. T., & Shearer, P. M. (2017). GrowClust: A hierarchical clustering algorithm for relative earthquake relocation, with application to the Spanish Springs and Sheldon, Nevada, earthquake sequences. *Seismological Research Letters*, *88*(2A), 379-391.

Tsai, Y., and K. Aki (1970), Source mechanism of the Truckee, California, earthquake of September 12 1966, *Bull. Seism. Soc. Am.* 60 (4), 1199-1208.

Twiss, S. R., and E. M. Moores (1992), *Structural Geology*, 532 pp., W. H. Freeman, New York.

von Seggern, D. H., J. G. Anderson, I. M. Tibuleac, and G. P. Biasi (2015), Double-Difference Location and Ground-Truth Classification of the 2008 Mogul, Nevada, Very Shallow Earthquake Sequence. *Seism. Res. Lett.* 86 *(1), 1-12.*

Wesnousky, S. G. (2005). Active faulting in the Walker Lane. *Tectonics*, *24*(3).

Wesnousky, S. G., J. M. Bormann, C. Kreemer, W. C. Hammond, and J. N. Brune (2012), Neotectonics, geodesy, and seismic hazard in the Northern Walker Lane of Western North America: Thirty kilometers of crustal shear and no strike-slip?, *Earth and Planetary Sci. Lett.* 329, 133-140.

Williams, C. F., & DeAngelo, J. (2011). Evaluation of approaches and associated uncertainties in the estimation of temperatures in the upper crust of the Western United States. GRC Transactions, 35, 1599-1605.

Zielke, O.,D. Schorlemmer, S. Jónsson, and P. M. Mai (2020). Magnitude-Dependent Transient Increase of Seismogenic Depth, Seismol. Res. Lett. 91, 2182–2191, doi: 10.1785/ 0220190392.

Zuza, A. V., & Cao, W. (2020). Seismogenic thickness of California: Implications for thermal structure and seismic hazard. *Tectonophysics*, 228426.

7 Figures

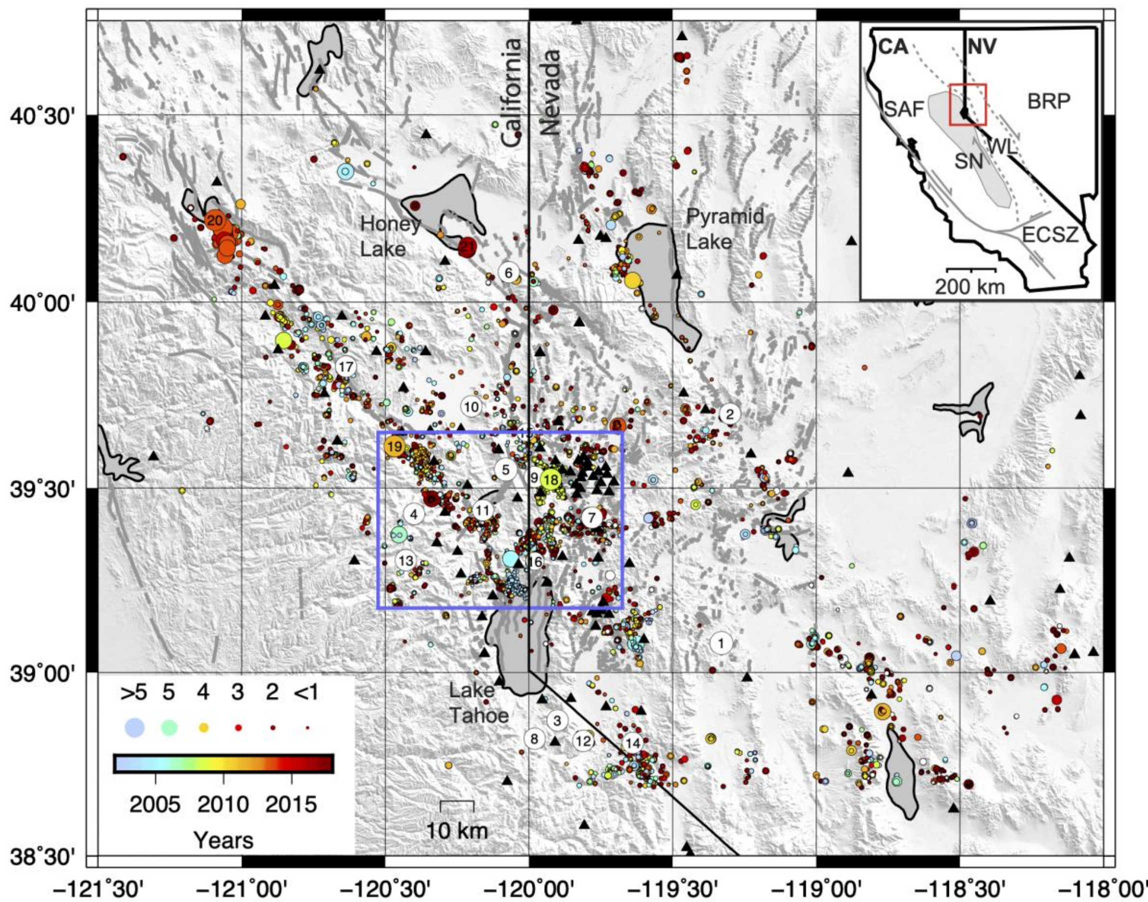

Figure 1. Earthquake location map of the study region, showing both historical seismicity in Table S1 (numbered events) and relocated microseismicity from 2002-2019 developed in this study. Seismicity is sized by magnitude and colored by time. Additionally, USGS Quaternary faults are shown as gray lines and regional seismic stations are shown by black triangles. Nevada (NV) and California (CA) are shown for geographical reference in the inset at top right. Significant tectonic features are labeled: the San Andreas fault system (SAF), Eastern California Shear Zone (ECSZ), Sierra Nevada block (SN), Walker Lane (WL), and Basin and Range province (BRP). Blue box shows area of maps in Figure 2.

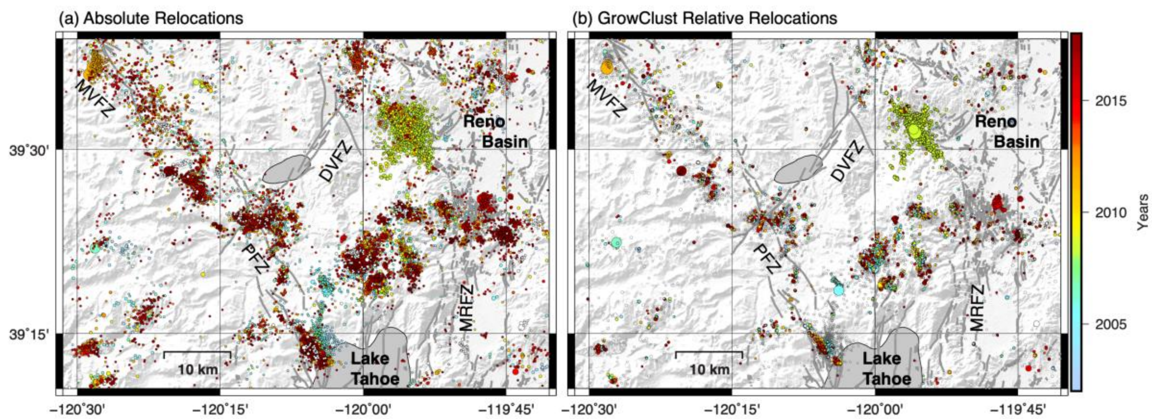

Figure 2. Maps of (a) absolute and (b) relative earthquake relocations in the Reno-Tahoe area with USGS Quaternary Faults plotted in gray. We label significant fault zones in the region for discussion purposes: Mohawk Valley Fault Zone (MVFZ; dextral), Dog Valley Fault Zone (DVFZ; sinistral), Polaris Fault Zone (PFZ; dextral), and Mount Rose Fault Zone (MRFZ; normal).

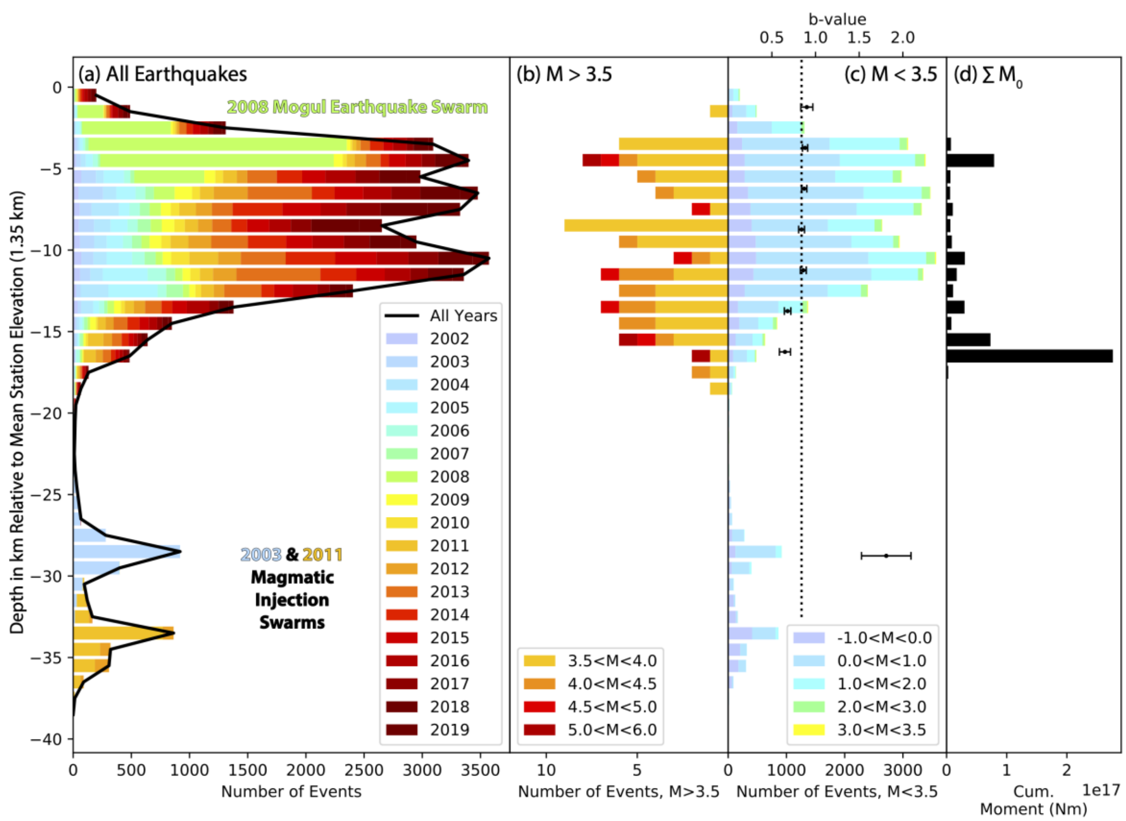

Figure 3. Histograms of seismogenic depth. (a) Depth distribution of all seismicity colored by time, (b) for M>3.5 earthquakes colored by magnitude, (c) for M<3.5 earthquakes colored by magnitude, and (d) by cumulative seismic moment. Frequency-magnitude b-value variation with depth is shown in (c). The dotted line shows overall b-value of 0.84 calculated for this dataset (see Figure S8), and the b-values for different depth ranges are plotted with error bars (black).

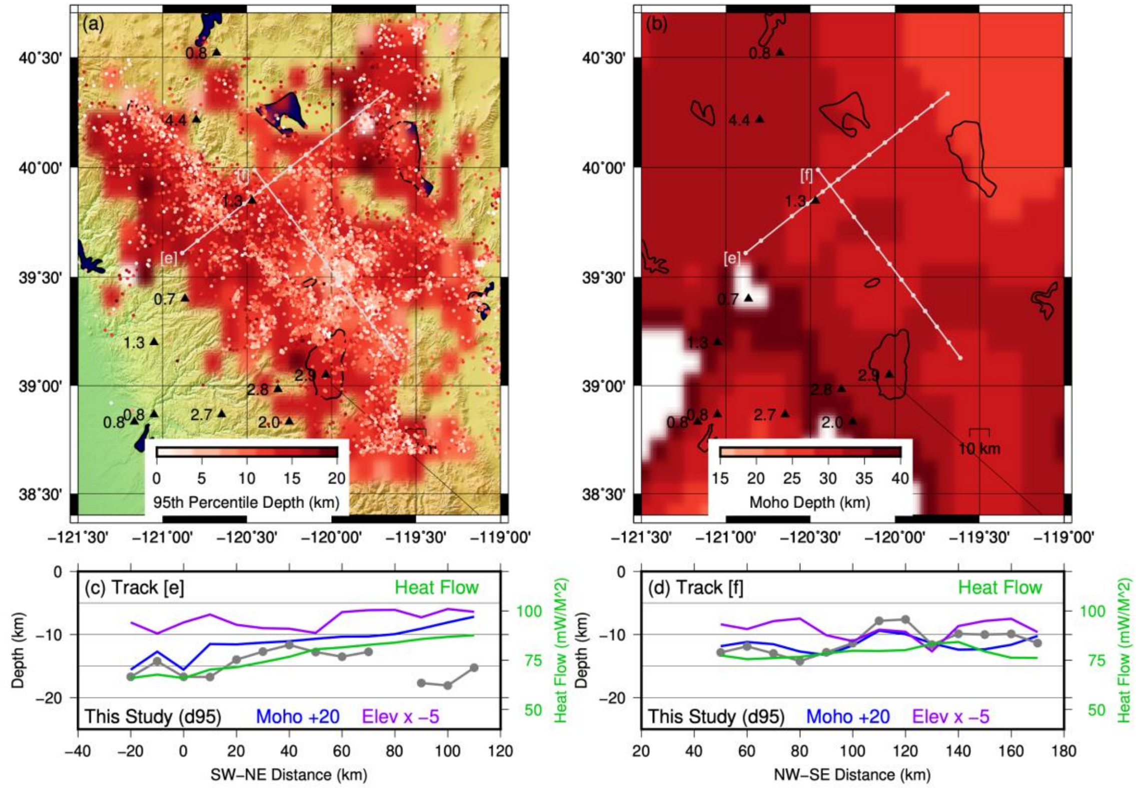

Figure 4. Comparison of seismogenic depth to Moho depth. (a) Map of relocated seismicity colored by depth plotted on top of our seismogenic depth grid using the same color scale. Triangles with numbers show geothermal temperatures from *Saltus & Lachenbruch* (1991). Light gray lines show profile lines for cross-sections (c) and (d). (b) Moho depth map with the same profiles and temperatures as shown in (a). Cross-sections for profile lines [e] and [f] are shown in (c) and (d), respectively. Seismogenic depth (gray lines with circles), Moho depth adjusted by 20 km to overlay the seismogenic depth (blue line), inverted and scaled elevations (purple lines), and heat flow (green lines) are shown in both. Moho depths from *Frasetto et al.* (2011) and heat flow measurements shown in tracks from *Willams and DeAngelo* (2011).